AEDC-TR-79-71

Computation of Axisymmetric Separated Nozzle-Afterbody Flow

J. L. Jacocks
ARO, Inc.

January 1980

Final Report for Period October 1, 1977 – July 30, 1979

Approved for public release; distribution unlimited.

ARNOLD ENGINEERING DEVELOPMENT CENTER
ARNOLD AIR FORCE STATION, TENNESSEE
AIR FORCE SYSTEMS COMMAND
UNITED STATES AIR FORCE

NOTICES
When U. S. Government drawings, specifications, or other data are used for any purpose other than a definitely related Government procurement operation, the Government thereby incurs no responsibility nor any obligation whatsoever, and the fact that the Government may have formulated, furnished, or in any way supplied the said drawings, specifications, or other data, is not to be regarded by implication or otherwise, or in any manner licensing the holder or any other person or corporation, or conveying any rights or permission to manufacture, use, or sell any patented invention that may in any way be related thereto.
Qualified users may obtain copies of this report from the Defense Technical Information Center.
References to named commerical products in this report are not to be considered in any sense as an indorsement of the product by the United States Air Force or the Government.

This report has been reviewed by the Office of Public Affairs (PA) and is releasable to the National Technical Information Service (NTIS). At NTIS, it will be available to the general public, including foreign nations.

APPROVAL STATEMENT

This report has been reviewed and approved.

Elton R Thompson

ELTON R. THOMPSON
Project Manager
Directorate of Technology

Approved for publication:

FOR THE COMMANDER

Marion L. Laster

MARION L. LASTER
Director of Technology
Deputy for Operations

REPORT DOCUMENTATION PAGE		READ INSTRUCTIONS BEFORE COMPLETING FORM
1. REPORT NUMBER AEDC-TR-79-71	2. GOVT ACCESSION NO.	3. RECIPIENT'S CATALOG NUMBER
4. TITLE (and Subtitle) COMPUTATION OF AXISYMMETRIC SEPARATED NOZZLE-AFTERBODY FLOW		5. TYPE OF REPORT & PERIOD COVERED Final Report, October 1, 1977 - July 30, 1979 6. PERFORMING ORG. REPORT NUMBER
7. AUTHOR(s) J. L. Jacocks, ARO, Inc., a Sverdrup Corporation Company		8. CONTRACT OR GRANT NUMBER(s)
9. PERFORMING ORGANIZATION NAME AND ADDRESS Arnold Engineering Development Center/DOT Air Force Systems Command Arnold Air Force Station, Tennessee 37389		10. PROGRAM ELEMENT, PROJECT, TASK AREA & WORK UNIT NUMBERS Program Element 65807F
11. CONTROLLING OFFICE NAME AND ADDRESS Arnold Engineering Development Center/DOS Arnold Air Force Station, Tennessee 37389		12. REPORT DATE January 1980 13. NUMBER OF PAGES 30
14. MONITORING AGENCY NAME & ADDRESS(if different from Controlling Office)		15. SECURITY CLASS. (of this report) UNCLASSIFIED 15a. DECLASSIFICATION/DOWNGRADING SCHEDULE N/A

16. DISTRIBUTION STATEMENT (of this Report)

Approved for public release; distribution unlimited.

17. DISTRIBUTION STATEMENT (of the abstract entered in Block 20, if different from Report)

18. SUPPLEMENTARY NOTES

Available in DTIC

19. KEY WORDS (Continue on reverse side if necessary and identify by block number)

computations	flow
computer program	turbulence
axisymmetric	viscosity
equations of motion	nozzle
calculations	afterbodies

20. ABSTRACT (Continue on reverse side if necessary and identify by block number)

The development of a computer program for solving the compressible, axisymmetric, mass-averaged Navier-Stokes equations is described. The basic numerical algorithm is the MacCormack explicit predictor-corrector scheme. Turbulence modeling is accomplished using an algebraic, two-layer eddy viscosity model with a novel modification dependent on the streamwise gradient of vorticity. Comparisons of computed results with experimental data

DD FORM 1 JAN 73 1473 EDITION OF 1 NOV 65 IS OBSOLETE

20. ABSTRACT (Continued)

are presented for several nozzle-afterbody configurations with either real or simulated plumes.

AFSC
Arnold AFS Tenn

PREFACE

The work reported herein was conducted by the Arnold Engineering Development Center (AEDC), Air Force Systems Command (AFSC). The Air Force project manager was Elton R. Thompson, DOT. The results of the research were obtained by ARO, Inc., AEDC Division (a Sverdrup Corporation Company), operating contractor for the AEDC, AFSC, Arnold Air Force Station, Tennessee, under ARO Projects No. P32A-P2A and P32A-01B. The manuscript was submitted for publication on September 19, 1979.

The author wishes to gratefully acknowledge Dr. George S. Deiwert, NASA, Ames Research Center, who furnished the basic planar Navier-Stokes computer program.

CONTENTS

ILLUSTRATIONS

1.0 INTRODUCTION

Current techniques for the prediction of propulsion system drag for aircraft rely heavily on wind tunnel tests. Yet, these tests do not incorporate complete simulation of the jet exhaust. Preliminary configuration tests in many cases use solid plume simulators (Ref. 1). Validation of the final design is accomplished in the wind tunnel with high-pressure air to simulate the nozzle exhaust flow. However, viscous interaction effects for a cold jet differ from those for a hot jet since mixing between the nozzle exhaust and local external flow depends largely on temperature, species, and velocity gradients. Experimental and analytical investigations at the Arnold Engineering Development Center (AEDC) (Refs. 2 through 6) have attempted to characterize the various simulation parameters necessary to obtain valid test results, but it is still not possible to accurately predict the afterbody drag on nozzle-afterbody models. If a sufficiently powerful analytical or numerical tool were available, the proper procedure for simulating a hot-jet exhaust flow with a cold fluid might be developed. Creation of this tool was the objective of the present investigation.

Current methods (Refs. 6 through 14, for example) for predicting nozzle-afterbody drag have relied on patched viscous-inviscid solutions wherein the complete flow field is computed in an iterative fashion, alternating between a potential flow solution and a viscous solution. With one notable exception (Ref. 14), these methods require severe under-relaxation of the viscous displacment correction, and the solutions obtained are unfortunately highly dependent on the relaxation technique. In spite of this difficulty, some of the methods are in good agreement with experimental data, particularly the method of Presz, King, and Buteau (Ref. 13).

Another approach to the afterbody problem is that of Holst (Ref. 15) who developed a numerical solution of the time-dependent, compressible Navier-Stokes equations. Holst demonstrated excellent agreement with surface pressure data obtained from experiments with circular-arc afterbodies and solid cylindrical plume simulators.

The present study is also based on numerical solution of the Navier-Stokes equations. The planar two-dimensional computer program developed by Deiwert (Ref. 16) was modified to enable computation of axisymmetric flow over nozzle afterbodies with either real or simulated plumes. The basic numerical algorithm is the explicit predictor-corrector scheme of MacCormack (Ref. 17). Turbulence modeling is accomplished using the algebraic, two-layer eddy viscosity model of Baldwin and Lomax (Ref. 18) with a novel local modification as a function of vorticity. The results presented are limited to comparisons of computations with the recent detailed flow-field measurements of Benek (Ref. 19) and with the surface data of Reubush (Ref. 1).

2.0 NUMERICAL METHOD

2.1 AXISYMMETRIC COMPRESSIBLE FLOW EQUATIONS

The equations describing the axisymmetric flow of a compressible, viscous fluid without body forces can be written in weak conservation form as follows (Refs. 20 and 21):

$$\frac{\partial rU}{\partial t} + \frac{\partial rF}{\partial x} + \frac{\partial rG}{\partial r} = A \tag{1}$$

where

$$U = \begin{bmatrix} \rho \\ \rho u \\ \rho v \\ E \end{bmatrix} \qquad F = \begin{bmatrix} \rho u \\ \rho u^2 + \sigma_x \\ \rho uv + \tau_{xr} \\ (E + \sigma_x)u + \tau_{xr}v + Q_x \end{bmatrix}$$

$$G = \begin{bmatrix} \rho v \\ \rho uv + \tau_{xr} \\ \rho v^2 + \sigma_r \\ (E + \sigma_r)v + \tau_{xr}u + Q_r \end{bmatrix} \qquad A = \begin{bmatrix} 0 \\ 0 \\ \sigma_\theta \\ 0 \end{bmatrix}$$

$$\sigma_x = P - \lambda \left(\frac{\partial u}{\partial x} + \frac{\partial v}{\partial r} \right) - 2(\mu + \epsilon) \frac{\partial u}{\partial x} - \frac{\lambda v}{r}$$

$$\sigma_r = P - \lambda \left(\frac{\partial u}{\partial x} + \frac{\partial v}{\partial r} \right) - 2(\mu + \epsilon) \frac{\partial v}{\partial r} - \frac{\lambda v}{r}$$

$$\tau_{xr} = -(\mu + \epsilon) \left(\frac{\partial u}{\partial r} + \frac{\partial v}{\partial x} \right)$$

$$\sigma_\theta = P - \lambda \left(\frac{\partial u}{\partial x} + \frac{\partial v}{\partial r} \right) - 2(\mu + \epsilon) \frac{v}{r} - \frac{\lambda v}{r}$$

$$Q_x = -\gamma \left(\frac{\mu}{Pr} + \frac{\epsilon}{Pr_T} \right) \frac{\partial e}{\partial x}$$

$$Q_r = -\gamma \left(\frac{\mu}{Pr} + \frac{\epsilon}{Pr_T} \right) \frac{\partial e}{\partial r}$$

The density, ϱ, is a mean value and the velocities, u and v, are mass-averaged values. The mass-averaged specific integral energy, e, is related to the mean total energy per unit volume, E, by

$$e = \frac{E}{\rho} - \tfrac{1}{2}\left(u^2 + v^2\right) \tag{2}$$

and the perfect gas equation of state

$$P = (\gamma - 1)\,\rho e \tag{3}$$

is used to define the mean pressure, P. The turbulence model (see Section 2.2) expresses the Reynolds stress tensor in terms of the scalar eddy viscosity, ϵ, which is additive to the molecular viscosity, μ, but not incorporated in the second coefficient of viscosity, λ, which is defined as $\lambda = -2/3\ \mu$. The Sutherland viscosity relation is used and the ratio of specific heats, γ, is maintained constant at 1.4. Laminar and turbulent Prandtl numbers are fixed at $Pr = 0.72$ and $Pr_T = 0.9$, respectively.

2.2 TURBULENCE MODEL

The two-layer algebraic turbulence model of Baldwin and Lomax (Ref. 18) was selected for this study because its use eliminates the necessity of locating the boundary-layer edge. The required length scale is determined from the distribution of vorticity in the vicinity of the body surface. The eddy viscosity, ϵ, is defined as a function of the normal distance from the wall, y, in the inner region as

$$\epsilon_{in} = \rho\, \ell^2\, |\omega| \tag{4}$$

and in the outer region as

$$\epsilon_{out} = KC_{CP}\rho\, F_{WAKE}\, F_{KLEB}(y) \tag{5}$$

The inner form is used out to the point where $\epsilon_{in} = \epsilon_{out}$ and from that point $\epsilon = \epsilon_{out}$. The auxiliary functions appearing in Eqs. (4) and (5) are defined as follows:

$$|\omega| = \left|\frac{\partial u}{\partial r} - \frac{\partial v}{\partial x}\right| \tag{6}$$

$$\ell = ky\left[1 - \exp\left(-y^+ / A^+\right)\right] \tag{7}$$

$$y^+ = \frac{y\sqrt{\rho_w \tau_w}}{\mu_w} \tag{8}$$

$$F_{KLEB}(y) = \left[1 + 5.5\left(\frac{C_{KLEB}\, y}{y_{MAX}}\right)^6\right]^{-1} \tag{9}$$

and

$$F_{WAKE} = y_{MAX} F_{MAX} \tag{10}$$

or

$$F_{WAKE} = C_{WK}\, y_{MAX}\, U_{DIF}^2 / F_{MAX}$$

whichever is the smallest, and the terms y_{MAX} and F_{MAX} are determined at the maximum of the function

$$F(y) = y\,|\omega|\left[1 - \exp\left(-y^+ / A^+\right)\right] \tag{11}$$

and

$$U_{DIF} = \left(\sqrt{u^2 + v^2}\right)_{MAX} - \left(\sqrt{u^2 + v^2}\right)_{MIN} \tag{12}$$

The constants appearing in this formulation are the following values assigned by Baldwin and Lomax:

$$A^+ = 26$$
$$C_{CP} = 1.6$$
$$C_{KLEB} = 0.3$$
$$C_{WK} = 0.25$$
$$k = 0.4$$
$$K = 0.0168$$

Holst (Ref. 15), Shang and Hankey (Ref. 22), and others have shown that turbulence models derived from turbulent boundary-layer data at equilibrium conditions do not yield good results when applied to separated flows. Their approach to introducing nonequilibrium effects was to arbitrarily select a streamwise location as a reference

condition and exponentially relax the calculated eddy viscosity through the separated region. This approach was included in the present analysis but yielded disappointing results.

One characteristic of boundary layers in equilibrium (observed in the present study) is that the streamwise gradient of vorticity is small. It follows, therefore, that the degree of nonequilibrium effects can be quantified by examining the vorticity gradient. This concept is used to locally adjust the Baldwin-Lomax eddy viscosity in the form

$$\epsilon_R = \epsilon \left(1 + \frac{\delta y_{MAX}}{|\omega|} \frac{d|\omega|}{dx}\right) \tag{13}$$

where δ is an arbitrary constant of order unity. As a matter of choice, the maximum change in ϵ is limited to $\pm$ 100 percent. This formulation, termed "vorticity gradient relaxation," is new and has not been fully explored.

2.3 SOLUTION ALGORITHM

For most practical situations the computational mesh is nonorthogonal and it is convenient to recast Eq. (1) into an integral form (Ref. 23) valid for each volume element as

$$\frac{\partial}{\partial t} \int_{Vol} rU \, dVol + \int_{S} r\vec{H} \cdot \vec{n} ds = \int_{Vol} A \, dVol \tag{14}$$

where $\vec{H}$ is the vector sum of F and G and $\vec{n}$ is the outward unit vector normal to the surface of the computational cell. The area vectors $\vec{n}ds$ are represented as $\vec{S}$ as shown in the sketch of an arbitrary quadrilateral volume element.

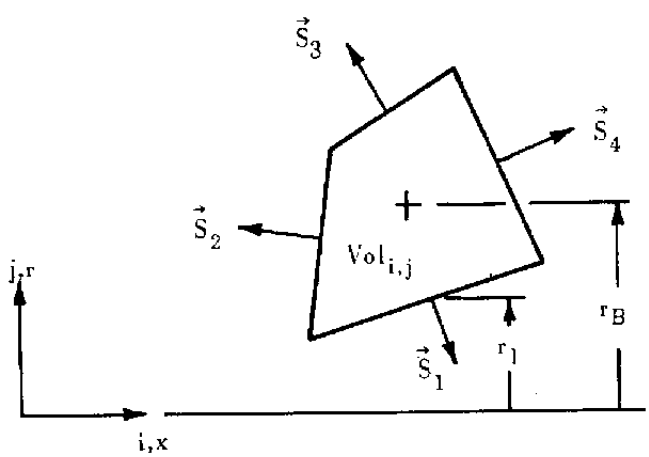

Early versions of the present formulation used the "splitting" technique of MacCormack and Paullay (Ref. 23) which worked quite well provided the mesh was aligned with the radial coordinate. Special applications, particularly inviscid solutions with irregular geometries, indicated that an unsplit solution procedure would be more stable and robust. The splitting technique was discarded, in spite of the time-saving attribute, because of pronounced oscillations in the dependent variables between predictor and corrector steps.

The MacCormack algorithm (Ref. 17) as applied to Eq. (14) may be written, with superscripts p and c representing predictor and corrector, as follows:

$$U^{p}_{i,j} = U_{i,j} - \frac{\Delta t}{r_B \, Vol}\left[r_1 \vec{H}_{1_{i,j-1}} \cdot \vec{S}_1 + r_2 \vec{H}_{2_{i-1,j}} \cdot \vec{S}_2 + r_3 \vec{H}_{3_{i,j}} \cdot \vec{S}_3 - v_4 \vec{H}_{4_{i,j}} \cdot \vec{S}_4 + A_{i,j}\, Vol\right]$$

$$U^{c}_{i,j} = \tfrac{1}{2}\left\{U_{i,j} + U^{p}_{i,j} - \frac{\Delta t}{r_B \, Vol}\left[r_1 \vec{H}^{p}_{1_{i,j}} \cdot S_1 + r_2 \vec{H}^{p}_{2_{i,j}} \cdot \vec{S}_2 + r_3 \vec{H}^{p}_{3_{i,j+1}} \cdot \vec{S}_3 + r_4 \vec{H}^{p}_{4_{i+1,j}} \cdot \vec{S}_4 + A^{p}_{i,j}\, Vol\right]\right\} \qquad (15)$$

The forward and backward permutations of the indices i,j are varied cyclically each time step (total of four steps) to balance the truncation error at each cell. Thus, the dependent variables U are explicitly advanced in time throughout the mesh to U^p, thence corrected to U^c.

The centroid radius, r_B, is currently the average of the radii at the cell corners. An earlier version of the program utilized the correct radial weighting to define r_B, but yielded no discernible difference relative to averaging.

The maximum allowable time step, Δt, is given by the Courant-Friedrich-Lewy (CFL) stability criteria, Ref. 21.

2.4 FINE-MESH CONSIDERATIONS

The CFL stability criteria require prohibitive computation time in regions of closely spaced mesh points which are necessary to resolve the viscous region adjacent to a surface. Again, recourse was made to MacCormack's initiative (Ref. 24) and Eq. (1) recast into time-split hyperbolic (inviscid) and parabolic parts. The hyperbolic equations are solved using an

explicit numerical method based on characteristic theory and the parabolic equations solved implicitly using a simple tridiagonal algorithm. The fine mesh is constrained to be stationary and parallel to the surface and Deiwert's (Ref. 25) local coordinate rotation incorporated to improve the solution accuracy.

Equation (1) is locally transformed from (x,r) to the surface-oriented (ξ,y) coordinates to yield

$$\frac{\partial rU}{\partial t} + \frac{1}{J}\left(\frac{\partial r}{\partial y}\frac{\partial rF}{\partial \xi} - \frac{\partial x}{\partial y}\frac{\partial rG}{\partial \xi}\right) + \frac{1}{J}\left(\frac{\partial x}{\partial \xi}\frac{\partial rG}{\partial y} - \frac{\partial r}{\partial \xi}\frac{\partial rF}{\partial y}\right) = A \tag{16}$$

where

$$J\left(\xi, y\right) = \frac{\partial x}{\partial \xi}\frac{\partial r}{\partial y} - \frac{\partial r}{\partial \xi}\frac{\partial x}{\partial y} = 1$$

Equation (16) is then split with the ξ-derivative terms handled as with Eq. (15) but the y-derivative terms further split into viscous and inviscid terms. The nomenclature associated with the coordinate rotation is defined in the following sketch

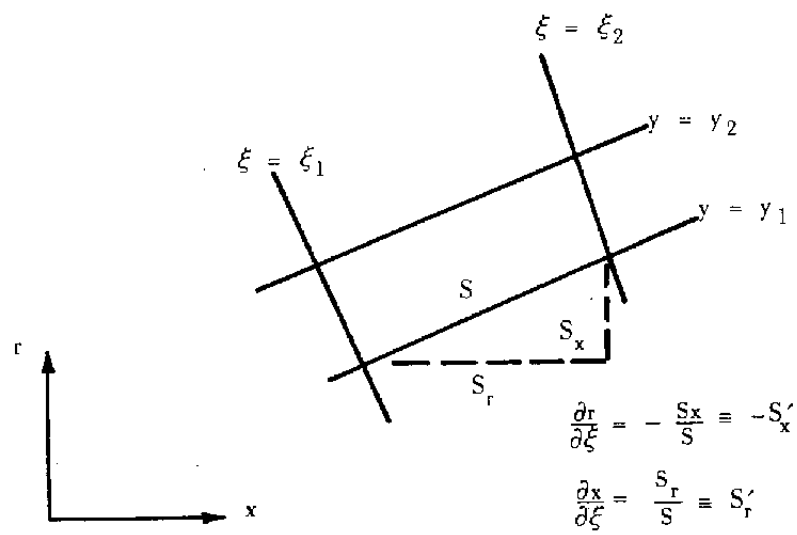

and tangential and normal velocity components defined as

$$u' = uS'_r - vS'_x$$

$$v' = uS'_x + vS'_r \tag{17}$$

The hyperbolic inviscid equations then may be written as

$$\frac{\partial \rho}{\partial t} + \frac{1}{JS}\frac{\partial \rho v'}{\partial y} = -\frac{\rho v}{r}$$

$$\frac{\partial \rho u}{\partial t} + \frac{1}{JS}\frac{\partial}{\partial y}\left(\rho u v' + S_x' P\right) = -\frac{\rho u v}{r}$$

$$\frac{\partial \rho v}{\partial t} + \frac{1}{JS}\frac{\partial}{\partial y}\left(\rho v v' + S_r' P\right) = -\frac{\rho v^2}{r}$$

$$\frac{\partial E}{\partial t} + \frac{1}{JS}\frac{\partial}{\partial y}\left[(E + P)\, v'\right] = -\frac{(E + P)\, v}{r} \tag{18}$$

which may be reduced to the form

$$\frac{\partial P}{\partial t} + \frac{\gamma P}{JS}\frac{\partial v'}{\partial y} + \frac{v'}{JS}\frac{\partial P}{\partial y} = -\frac{\gamma P v}{r}$$

$$\frac{\partial v'}{\partial t} + \frac{v'}{JS}\frac{\partial v'}{\partial y} + \frac{1}{\rho JS}\frac{\partial P}{\partial y} = 0$$

$$\frac{\partial u'}{\partial t} + \frac{v'}{JS}\frac{\partial u'}{\partial y} = 0 \tag{19}$$

where the continuity and energy equations are redundant. For small v', the last expresssion of Eq. (19) may be temporarily neglected to obtain characteristic relations

$$J\frac{dy}{dt} = v' \pm c$$

$$\frac{1}{\rho}\frac{dP}{dt} + \frac{c^2 v}{r} \pm c\frac{dv'}{dt} = 0 \tag{20}$$

where the speed of sound is given by

$$c = \left[\frac{\gamma P}{\rho}\right]^{1/2} \tag{21}$$

The normal velocity, v', and pressure, P, are provisionally advanced in time using the characteristic relations (evaluating the term $c^2 v/r$ at the previous time value), the tangential velocity is updated via the last expression of Eq. (19), and the density is updated using $d\rho = dP/c^2$. These estimated variables are then used to calculate the inviscid flux vectors $\vec{H}_1 \cdot \vec{S}_1$ and $\vec{H}_3 \cdot \vec{S}_3$ of Eq. (15) which are held fixed during both the predictor and corrector steps.

The parabolic viscous equations may be written as

$$\frac{\partial \rho}{\partial t} = 0$$

$$\frac{\partial u'}{\partial t} = -\frac{1}{r\rho J}\frac{\partial}{\partial y}\left\{r\bar{\sigma}_x S_x' S_r' + r\tau_{xr}\left(S_r' S_r' - S_x' S_x'\right) - r\bar{\sigma}_r S_r' S_x'\right\} - \frac{S_x' \bar{\sigma}_\theta}{r\rho}$$

$$\frac{\partial v'}{\partial t} = -\frac{1}{r\rho J}\frac{\partial}{\partial y}\left\{r\bar{\sigma}_x S_x' S_x' + 2r\tau_{xr} S_x' S_r' + r\bar{\sigma}_r S_r' S_r'\right\} + \frac{Sy' \bar{\sigma}_\theta}{r\rho}$$

$$\frac{\partial E/\rho}{\partial t} = -\frac{1}{r\rho J}\frac{\partial}{\partial y}\left\{rS_x'\left(\bar{\sigma}_x u + \tau_{xr} v - Q_x\right) + rS_r'\left(\tau_{xy} u + \bar{\sigma}_r v - Q_y\right)\right\} \tag{22}$$

where the continuity equation is represented by stationary density (and $\bar{\sigma}_x = \sigma_x - P$, etc.). The momentum equations may be rearranged to yield

$$\frac{\partial u'}{\partial t} = \frac{1}{r\rho JS}\frac{\partial rT_1}{\partial y} - \frac{S_x' \bar{\sigma}_\theta}{r\rho}$$

$$\frac{\partial v'}{\partial t} = \frac{1}{r\rho JS}\frac{\partial rT_2}{\partial y} + \frac{S_r' \bar{\sigma}_\theta}{r\rho} \tag{23}$$

where

$$T_1 = \frac{S(\mu + \epsilon)}{J}\frac{\partial u'}{\partial y} + \frac{S(\mu + \epsilon)}{J}\left\{\frac{\partial x}{\partial y}\frac{\partial u}{\partial \xi} + \frac{\partial r}{\partial y}\frac{\partial v}{\partial \xi} + 2\left(S_r'\frac{\partial u}{\partial \xi} - S_x'\frac{\partial v}{\partial \xi}\right)\left(S_x'\frac{\partial r}{\partial y} - S_r'\frac{\partial x}{\partial y}\right)\right\}$$

$$T_2 = \left(\lambda + 2(\mu + \epsilon)\right)\frac{S}{J}\frac{\partial v'}{\partial y} + \frac{\lambda S}{J}\left(\frac{\partial r}{\partial y}\frac{\partial u}{\partial \xi} - \frac{\partial x}{\partial y}\frac{\partial v}{\partial \xi}\right) + \frac{v\lambda S}{r} + \frac{2(\mu + \epsilon)S}{J}\left(S_x'\frac{\partial r}{\partial y} - S_r'\frac{\partial x}{\partial y}\right)\left(S_x'\frac{\partial u}{\partial \xi} + S_r'\frac{\partial v}{\partial \xi}\right)$$

These equations are solved numerically (see Ref. 24) using first-order Laasonen implicit differencing and tridiagonal reduction. The energy equation is replaced by two kinetic energy relations and an internal-energy equation written as

$$\frac{\partial u'^2}{\partial t} = \frac{2}{r\rho SJ}\left(\frac{\partial r u' T_1}{\partial y} - r T_1 \frac{\partial u'}{\partial y}\right)$$

$$\frac{\partial v'^2}{\partial t} = \frac{2}{r\rho SJ}\left(\frac{\partial r v' T_2}{\partial y} - r T_2 \frac{\partial v'}{\partial y}\right) + \frac{2 S_r' v' \bar{\sigma}_\theta}{r\rho}$$

$$\frac{\partial e}{\partial t} = \frac{1}{r\rho SJ}\frac{\partial}{\partial y}\left\{\frac{r}{J}\left[\left(\frac{\gamma\mu}{Pr} + \frac{\gamma\epsilon}{Pr_T}\right)\left(S\frac{\partial e}{\partial y} + S\frac{\partial e}{\partial \xi}\right)\left(S_x'\frac{\partial r}{\partial y} - S_r'\frac{\partial x}{\partial y}\right)\right]\right\}$$

$$+ \frac{1}{\rho SJ}\left(T_1\frac{\partial u'}{\partial y} + T_2\frac{\partial v'}{\partial y}\right) - \frac{v\bar{\sigma}_\theta}{r\rho} \qquad (24)$$

Solution of Eq. (24) requires only one additional tridiagonal reduction.

The solution of the fine mesh is advanced in time using basically two operators in the sequence $L_1(\Delta t/2)L_2(\Delta t)L_1(\Delta t/2)$. The operator L_1 is Eq. (15) without the viscous terms in the "j" direction (unsplit) and the operator L_2 is the implicit split viscous solution, Eqs. (23) and (24).

2.5 SMOOTHING

Two types of smoothing are incorporated to eliminate "wiggles." The basic MacCormack algorithm is subject to nonlinear stability problems and his expansion-averaging technique (Ref. 26) is used to maintain stability. The second type of smoothing used was also suggested by MacCormack and consists of explicitly including some of the third-order truncation errors in evaluating the flux vectors $\vec{H} \cdot \vec{S}$ in Eq. (15).

The source of the third-order smoothing terms may be seen by considering the following model nonlinear equation

$$\frac{\partial f}{\partial t} + \frac{\partial f g}{\partial x} = 0 \qquad (25)$$

with

$$f = f(x,t)$$

$$g = g(f)$$

and applying the MacCormack algorithm in the form

$$f_i^p = \bar{f}_i = f_i - \frac{\Delta t}{\Delta x}\left[(fg)_{i+1} - (fg)_i\right]$$

$$f_i^c = f_i^{n+1} = \tfrac{1}{2}\left\{f_i + \bar{f}_i - \frac{\Delta t}{\Delta x}\left[(\bar{f}g)_i - (\bar{f}g)_{i-1}\right]\right\} \tag{26}$$

The solution is considered exact at time n and Taylor series expansions in the form

$$(fg)_{i+1} = (fg)_i + \Delta x \frac{\partial fg}{\partial x} + \frac{\Delta x^2}{2!}\frac{\partial^2 fg}{\partial x^2} + \frac{\Delta x^3}{3!}\frac{\partial^3 fg}{\partial x^3}$$

$$(\bar{f}g)_{i-1} = (\bar{f}g)_i - \Delta x \frac{\partial \bar{f}g}{\partial x} + \frac{\Delta x^2}{2!}\frac{\partial^2 \bar{f}g}{\partial x^2} - \frac{\Delta x^3}{3!}\frac{\partial^3 \bar{f}g}{\partial x^3}$$

$$\bar{g}_i = g_i + (\bar{f}_i - f_i)\frac{\partial g}{\partial f} + \frac{(\bar{f}_i - f_i)^2}{2!}\frac{\partial^2 g}{\partial f^2} + \frac{(\bar{f}_i - f_i)^3}{3!}\frac{\partial^3 g}{\partial f^3} \tag{27}$$

are used to evaluate the error encountered at time n + 1 by comparison with the Taylor series expansion of the exact solution. Defining

$$\phi = f\frac{dg}{df} + g \tag{28}$$

the MacCormack algorithm yields

$$f_i^{n+1} = f_i - \Delta t \frac{\partial fg}{\partial x} + \frac{\Delta t^2}{2}\frac{\partial}{\partial x}\left(\phi \frac{\partial fg}{\partial x}\right)$$

$$- \frac{\Delta t^3}{4}\frac{\partial}{\partial x}\left(\frac{\partial \phi}{\partial f}\left(\frac{\partial fg}{\partial x}\right)^2\right) - \frac{\Delta t^2 \Delta x}{4}\frac{\partial}{\partial x}\left(\phi \frac{\partial^2 fg}{\partial x^2}\right)$$

$$- \frac{\Delta t^2 \Delta x}{2}\frac{\partial}{\partial x}\left(\frac{\partial \phi}{\partial x}\frac{\partial fg}{\partial x}\right) - \frac{\Delta t \Delta x^2}{6}\frac{\partial^3 fg}{\partial x^3} + o\left(\Delta t^4\right) \tag{29}$$

and the exact solution is

$$f(t + \Delta t) = f - \Delta t \frac{\partial fg}{\partial x} + \frac{\Delta t^2}{2}\frac{\partial}{\partial x}\left(\phi \frac{\partial fg}{\partial x}\right)$$

$$- \frac{\Delta t^3}{6}\frac{\partial}{\partial x}\left(\frac{\partial \phi}{\partial f}\left(\frac{\partial fg}{\partial x}\right)^2\right) - \frac{\Delta t^3}{6}\phi \frac{\partial}{\partial x}\left(\phi \frac{\partial^2 fg}{\partial x^2}\right)$$

$$- \frac{\Delta t^3}{6}\phi \frac{\partial}{\partial x}\left(\frac{\partial \phi}{\partial x}\frac{\partial fg}{\partial x}\right) - \frac{\Delta t^3}{6}\left(\frac{\partial \phi}{\partial x}\right)^2 \frac{\partial fg}{\partial x} - \frac{\Delta t^3}{6}\phi \frac{\partial \phi}{\partial x}\frac{\partial^2 fg}{\partial x^2} + o\left(\Delta t^4\right) \tag{30}$$

Comparison of these expressions shows that MacCormack's algorithm on a uniform mesh is second-order accurate for this class of nonlinear equations. Indeed, much of the "flavor" of the third-order terms is present and, with $\Delta x = \phi \Delta t$, the truncation error at third order is given approximately by

$$f_i^{n+1} - f(t + \Delta t) = \frac{\Delta t^3}{6}\left(\frac{\partial \phi}{\partial x}\right)^2 \frac{\partial f_g}{\partial x} + \frac{\Delta t^3}{6} \frac{\partial \phi}{\partial x} \frac{\partial^2 f_g}{\partial x^2} - \frac{\Delta t^3}{6} \phi^2 \frac{\partial^3 f_g}{\partial x^3} \tag{31}$$

Since these terms are small it is not necessary to code them exactly and note simply that the truncation errors are proportional to the first, second, and third spatial derivatives. In practice, the CFL stability criterion for the split Euler equations define the relationship between Δt and Δx which specifies $\phi = |u| + c$ or $|v| + c$.

2.6 COMPUTATIONAL MESH AND BOUNDARY CONDITIONS

Representative mesh constructions are given in Fig. 1. A fine exponentially stretched mesh is constrained to be parallel to the body surface and extends into the wake/plume region, if present, as shown in Fig. 1b with the first node point within the viscous sublayer. Coarser mesh point spacing is specified in regions of reduced viscous effects with radial exponential stretching in the outer flow and proportionate radial spacing within the plume. The mesh includes points at the boundaries for specification of boundary conditions.

Zero-slip boundary conditions at viscous surfaces are applied using the reflection principle on velocities, evaluation of the normal momentum equation for pressure, adiabatic wall conditions for internal energy, and the equation of state for density. Inflow boundary conditions are fixed in time at the initial condition as is the upper boundary condition. The outflow or downstream boundary condition is updated assuming zero gradients in the streamwise direction and the centerline, if present, is treated with symmetry.

Initial conditions consist of uniform flow everywhere in the coarse mesh and a boundary-layer-type profile in the fine mesh obtained from Whitfield's velocity profile (Ref. 27) with specification of the desired inflow boundary-layer displacement and momentum thicknesses. For the real-plume calculations, the interior inflow is computed from isentropic relations with stagnation pressure and temperature being smoothly varied to the desired conditions over the first 100 time steps.

3.0 RESULTS AND DISCUSSION

3.1 FLOW OVER A BOATTAIL WITH SIMULATED PLUME

Benek (Ref. 19) has recently completed an experimental investigation specifically designed to provide information for the validation of axisymmetric-flow computer programs. The geometry used in that program is represented in Fig. 1a and consists of a circular-arc boattail ($\ell/D = 0.8$) followed by a contoured solid plume simulator. Detailed flow-field measurements using laser velocimetry were made including results at locations corresponding to the boundary of the computational domain.

Computed results from the present analysis are compared with Benek's data in Figs. 2 and 3. The surface pressure comparison (Fig. 2) shows good agreement except in the vicinity of the cusp where separated flow is evident. (If the measurements were to be adjusted from the stated $M_\infty = 0.64$ to an apparent free-stream Mach number of 0.635, then the computations and data would be in excellent agreement upstream of the boattail.) Application of vorticity-gradient relaxation ($\delta = 2$) to the Baldwin-Lomax turbulence model ($\delta = 0$) significantly changes the computed results. The effect of relaxation is vividly shown in the velocity profile comparisons given in Fig. 3. Relaxation improves the solution at some locations (at separation and reattachment in particular) but has adverse effects at other stations. It is obvious that the turbulence model could be tuned to yield computed results in complete agreement with this experimental data, and equally obvious that the turbulence model is the weakest link in the computation of turbulent separated flow.

3.2 EFFECT OF THIRD-ORDER SMOOTHING

The flow field about the boattail is presented in Fig. 4 in the form of isobars to illustrate the smoothing achieved by explicit consideration of the third-order truncation errors. The "wiggles" evident in Fig. 4a are suppressed in Fig. 4b by including the gradient smoothing term, $\partial fg/\partial x$, of Eq. (31). Although not shown, the gradient term is particularly effective in smoothing a solution containing embedded shock waves. Further addition of the curvature smoothing term, $\partial^2 fg/\partial x^2$, suppresses the wiggles over the cusp region as shown in Fig. 4c. Since this solution is sufficiently smooth, the third derivative term was not included in the computer program. A note of caution is in order — this type of smoothing is so powerful that wiggles arising from coding errors can also be smoothed.

3.3 FLOW OVER A BOATTAIL WITH REAL PLUME

Reubush (Ref. 1) presents surface data for a variety of boattails with and without cylindrical plume simulators. One configuration (No. 1) was selected for comparison with the present program and the results are given in Fig. 5. The pressure distribution over the boattail is reasonably well predicted but it is not known to what degree of accuracy the plume is calculated. The computed velocity vectors at the nozzle exit are given in Fig. 6 to illustrate the flow-field complexity. It is highly desirable that some agency obtain detailed experimental measurements about this type of nozzle afterbody with a real plume to provide code verification data. Modeling of the mixing and entrainment effects of the plume cannot be accomplished by comparison with surface pressure data alone.

4.0 CONCLUDING REMARKS

A generalized axisymmetric version of Deiwert's compressible Navier-Stokes computer program has been developed. The immediate objective was the generation of a tool for the prediction of jet simulation parameters to be used in wind tunnel tests of nozzle-afterbody configurations. Limited comparisons of computed results with experimental data indicate that the perfection of such a tool awaits solution of the turbulence modeling problem. Nonetheless, for a given turbulence model it is expected that the computer program can be used to reasonably well predict the incremental effects on nozzle-afterbody drag as influenced by internal geometry, nozzle pressure ratio, and exhaust temperature.

REFERENCES

1. Reubush, D. E. "Experimental Study of the Effectiveness of Cylindrical Plume Simulators for Predicting Jet-On Boattail Drag at Mach Numbers up to 1.30." NASA TN D-7795, November 1974.

2. Robinson, C. E. and High, M. D. "Exhaust Plume Temperature Effects on Nozzle Afterbody Performance over the Transonic Mach Number Range." AEDC-TR-74-9 (AD781377), July 1974.

3. Robinson, C. E. "Evaluation of Reynolds Number and Tunnel Wall Porosity Effects on Nozzle Afterbody Drag at Transonic Mach Numbers." AEDC-TR-76-70 (ADA027388), July 1976.

4. Galigher, L. L., Yaros, S. F., and Bauer, R. C. "Evaluation of Boattail Geometry and Exhaust Plume Temperature Effects on Nozzle Afterbody Drag at Transonic Mach Numbers." AEDC-TR-76-102 (ADA030852), October 1976.

5. Peters, W. L. "An Evaluation of Jet Simulation Parameters for Nozzle Afterbody Testing at Transonic Mach Numbers." AEDC-TR-76-109 (ADA031525), October 1976.

6. Yaros, S. F. "Prediction of Pressure Distributions on Axisymmetric Bodies in Transonic Flow." AIAA Paper No. 77-226, January 1977.

7. Chow, W. L., Bober, L. J., and Anderson, B. H. "Numerical Calculation of Transonic Boattail Flow." NASA TN D-7984, June 1975.

8. Reubush, D. E. and Putnam, L. E. "An Experimental and Analytical Investigation of the Effect on Isolated Boattail Drag of Varying Reynolds Number up to 130 x 10^6." NASA TN D-8210, May 1976.

9. Wilmoth, R. G. "Analytical Study of Viscous Effects on Transonic Flow over Boattail Nozzles." AIAA Paper No. 77-223, January 1977.

10. Cosner, R. R. and Bower, W. W. "A Patched Solution of the Transonic Flowfields About An Axisymmetric Boattail." AIAA Paper No. 77-227, January 1977.

11. Yaeger, L. S. "Transonic Flow Over Afterbodies Including the Effects of Jet-Plume and Viscous Interactions with Separation." AIAA Paper No. 77-228, January 1977.

12. Wilmoth, R. G. "Computation of Transonic Boattail Flow with Separation." NASA TP-1070, December 1977.

13. Presz, W. M., Jr., King, R. W., and Buteau, J. D. "An Improved Analytical Model of the Separation Region on Boattail Nozzles at Subsonic Speeds." NASA CR-3028, July 1978.

14. Carter, J. E. "A New Boundary-Layer Interaction Technique for Separated Flows." NASA TM-78690, June 1978.

15. Holst, T. L. "Numerical Solution of Axisymmetric Boattail Fields with Plume Simulators." AIAA Paper No. 77-224, January 1977.

16. Deiwert, G. S. "Numerical Simulation of High Reynolds Number Transonic Flows." AIAA Paper No. 74-603, June 1974.

17. MacCormack, R. W. "The Effect of Viscosity in Hypervelocity Impact Cratering." AIAA Paper No. 69-354, May 1969.

18. Baldwin, B. S. and Lomax, H. "Thin Layer Approximation and Algebraic Model for Separated Turbulent Flows." AIAA Paper No. 78-257, January 1978.

19. Benek, J. A. "Separated and Nonseparated Turbulent Flows About Axisymmetric Nozzle Afterbodies." AEDC-TR-79-22, 1979.

20. Rubesin, M. W. and Rose, W. C. "The Turbulent Mean-Flow, Reynolds-Stress, and Heat-Flux Equations in Mass-Averaged Dependent Variables." NASA TM X-62,248, March 1973.

21. Baldwin, B. S., MacCormack, R. W., and Deiwert, G. S. "Numerical Techniques for the Solution of the Compressible Navier-Stokes Equations and Implementation of Turbulence Models." AGARD LS-73, February 1975.

22. Shang, J. S. and Hankey, W. L., Jr. "Numerical Solution for Supersonic Turbulent Flow Over a Compression Ramp." *AIAA Journal*, Vol. 13, No. 10, October 1975.

23. MacCormack, R. W. and Paullay, A. J. "Computational Efficiency Achieved by Time Splitting of Finite Difference Operators." AIAA Paper No. 72-154, January 1972.

24. MacCormack, R. W. "An Efficient Numerical Method for Solving the Time-Dependent Compressible Navier-Stokes Equations at High Reynolds Number." NASA TM X-73, 129, July 1976.

25. Deiwert, G. S. "Computation of Turbulent Separated Flow." Lecture Notes for Short Course on Advances in Computational Fluid Dynamics, The University of Tennessee Space Institute, Tullahoma, Tennessee, December 1978.

26. MacCormack, R. W. "Numerical Solutions of the Interaction of a Shock Wave with a Laminar Boundary Layer." Lecture Notes in Physics, Vol. 8, Springer-Verlag, New York, 1971.

27. Whitfield, D. L. "Analytical Description of the Complete Two-Dimensional Turbulent Boundary-Layer Velocity Profile." AEDC-TR-77-79 (ADA045033), September 1977.

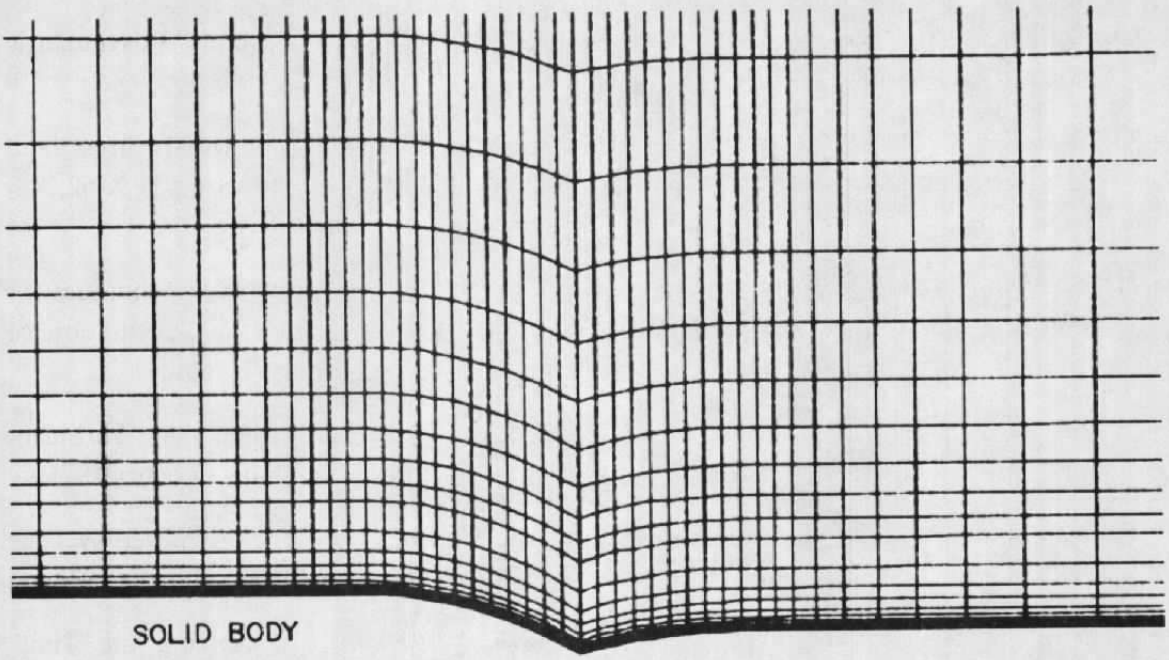

a. Simulated plume

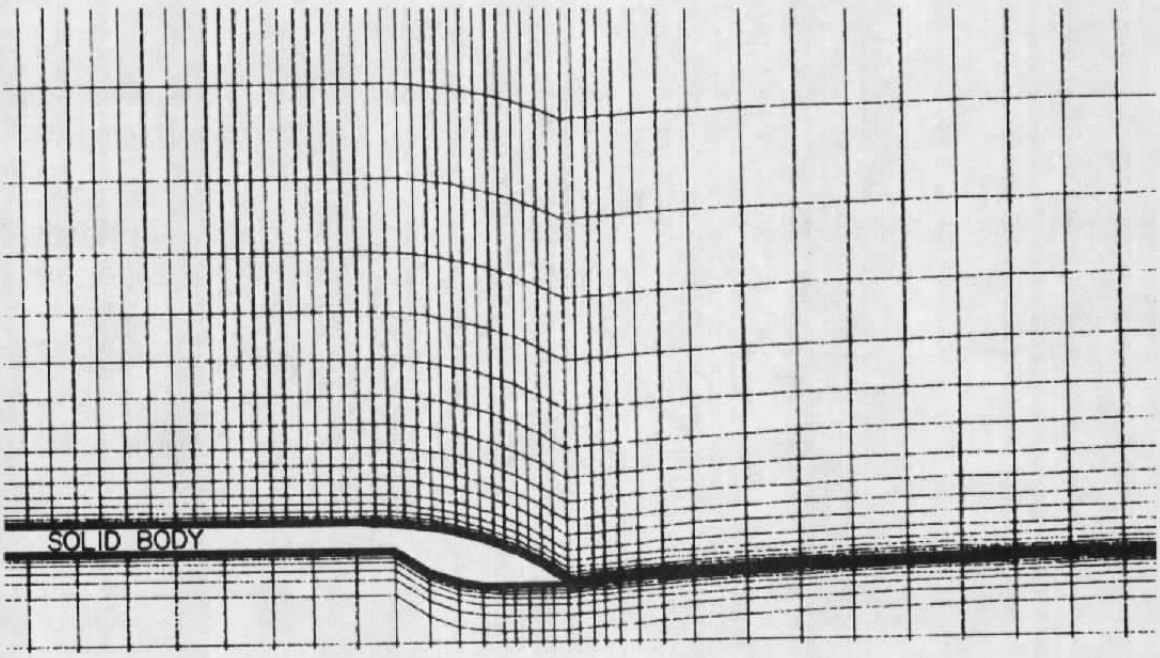

b. Real plume

Figure 1. Representative computational meshes.

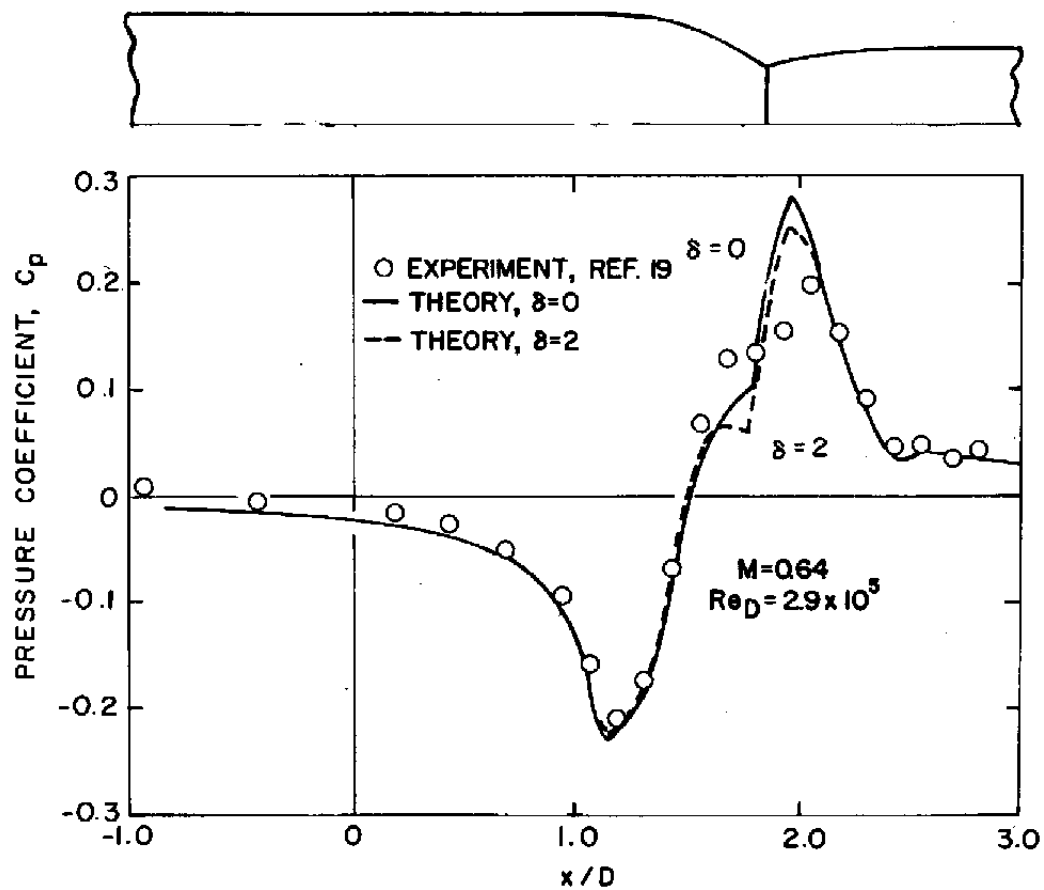

Figure 2. Comparison of computed and measured surface pressure coefficients on an afterbody with simulated plume.

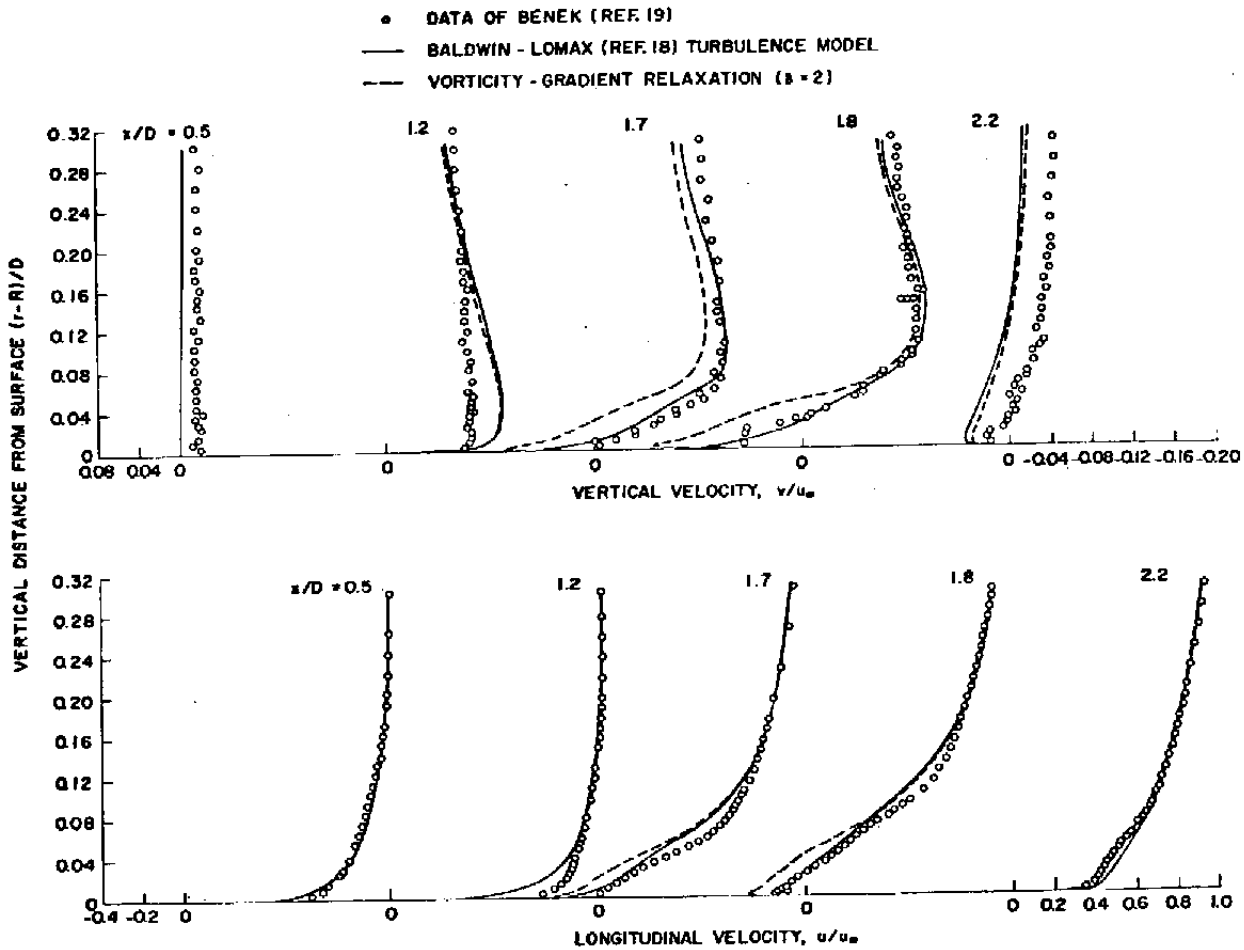

Figure 3. Comparison of computed and measured velocity profiles about an afterbody with simulated plume.

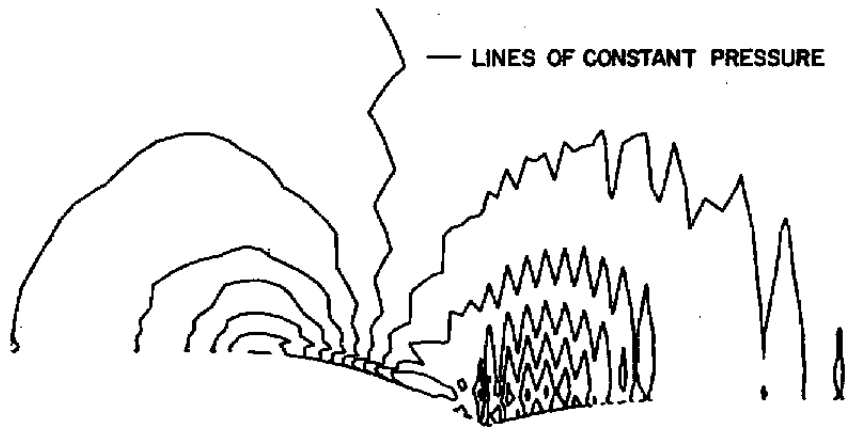

a. Expansion-averaging only

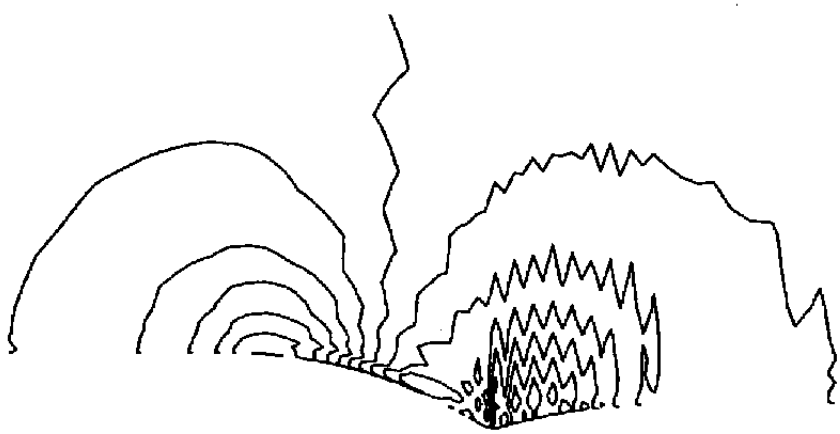

b. Gradient smoothing

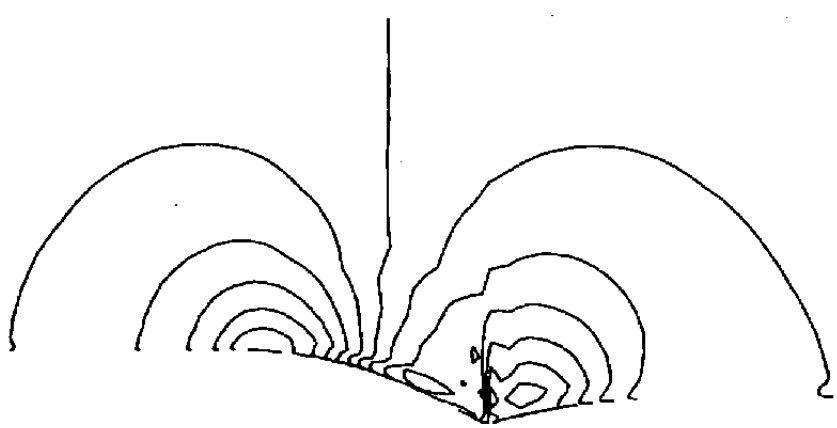

c. Curvature smoothing

Figure 4. Effect of third-order smoothing.

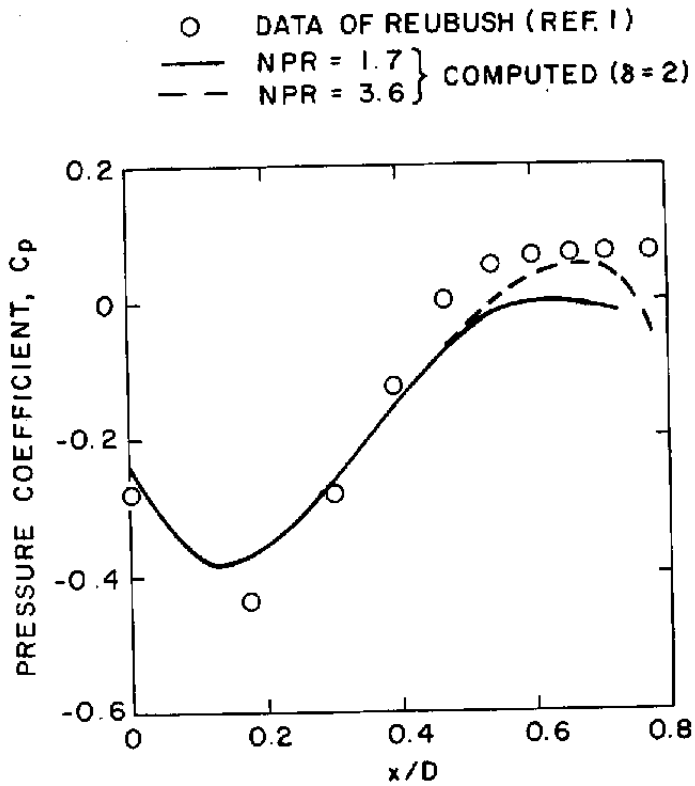

Figure 5. Comparison of computed and measured surface pressure coefficients on an afterbody with real plume, $M_\infty = 0.8$.

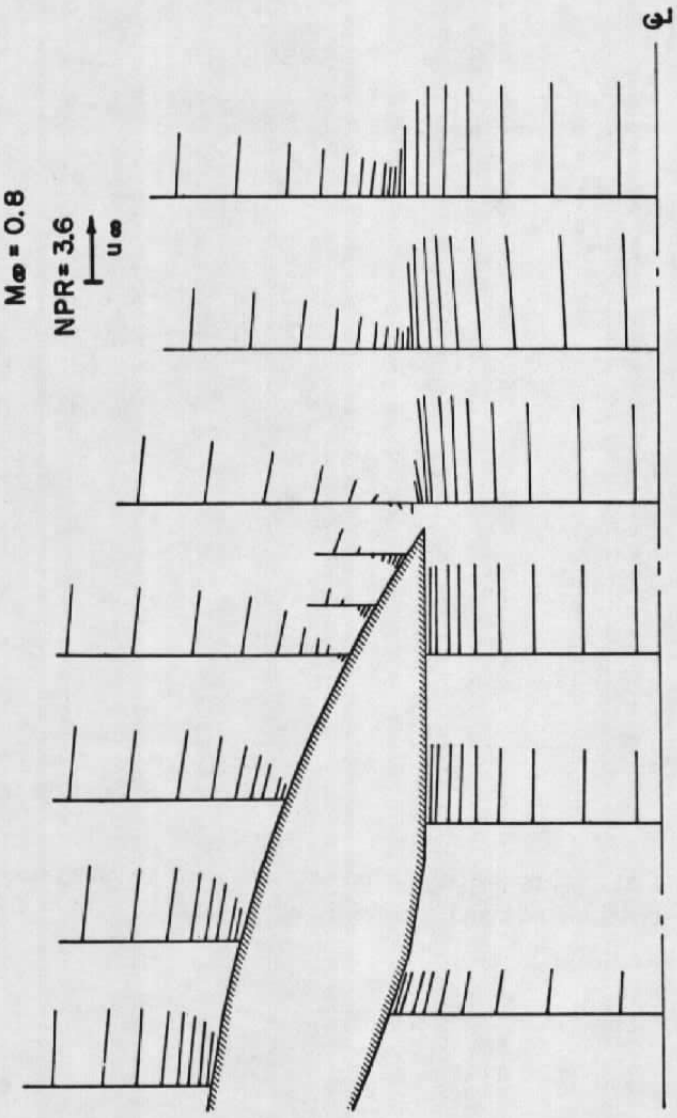

Figure 6. Velocity vectors at exit of a nozzle-afterbody.

NOMENCLATURE

A	Source term in Eq. (1), also van Driest's constant
c	Speed of sound, also model chord
C_{CP}	Turbulence model Baldwin-Lomax constant (see Eq. (5))
C_{KLEB}	Turbulence model Klebanoff constant (see Eq. (9))
C_p	Pressure coefficient, $(P-P_\infty)/q_\infty$
C_{WK}	Turbulence model wake constant (see Eq. (10))
D	Model diameter
E	Mean total energy per unit volume
e	Specific internal energy
F	See Eq. (1)
F_{KLEB}	Turbulence model (see Eq. (9))
F_{MAX}	Turbulence model (see Eq. (11))
F_{WAKE}	Turbulence model (see Eq. (10))
f	General functional
G	See Eq. (1)
g	General functional
J	Jacobian
K	Turbulence model constant
k	Turbulence model constant
ℓ	Turbulence model mixing length, also model length
M	Mach number
$\vec{n}$	Unit normal vector
P	Static pressure
Pr	Prandtl number, laminar

Pr_T	Prandtl number, turbulent
Q	Heat
q	Dynamic pressure
R	Model radius
Re	Unit Reynolds number
r	Radial coordinate
S	Surface area
$\vec{s}$	Directed surface area
T_1, T_2	See Eq. (23)
t	Time
U	See Eq. (1)
U_{DIF}	Turbulence model function (see Eq. (12))
u	Longitudinal velocity
Vol	Volume
v	Radial velocity
x	Longitudinal coordinate
y	Normal coordinate
y_{MAX}	Turbulence model function (see Eq. (11))
γ	Ratio of specific heats
Δr	Radial increment
Δt	Time increment
Δx	Longitudinal increment
δ	Vorticity-gradient relaxation parameter (see Eq. (13))
ϵ	Eddy viscosity

ϵ_R	Relaxed eddy viscosity
λ	Second coefficient of viscosity
μ	First coefficient of viscosity
ξ	Tangential coordinate
ϱ	Density
σ	Normal stress including pressure
$\bar{\sigma}$	Normal stress excluding pressure
τ	Tangential stress
ϕ	See Eq. (28)
ω	Vorticity

SUBSCRIPTS

B	Denotes mesh cell centroid
c	Denotes reference to model chord
D	Denotes reference to model diameter
i	Numerical index
in	Denotes reference to inner portion
j	Numerical index
out	Denotes reference to outer portion
r	Deontes radial direction
w	Denotes wall conditions
x	Denotes longitudinal direction
θ	Denotes circumferential direction
∞	Denotes free-stream conditions